Clin Oral Invest (2013) 17:285–292
DOI 10.1007/s00784-012-0688-2

ORIGINAL ARTICLE

Reproducibility of three-dimensional cephalometric landmarks in cone-beam and low-dose computed tomography

R. Olszewski · L. Frison · M. Wisniewski · J. M. Denis · S. Vynckier · G. Cosnard · F. Zech · H. Reychler

Received: 3 December 2010 / Accepted: 31 January 2012 / Published online: 17 February 2012

Abstract
Objectives The purpose of this study is to compare the reproducibility of three-dimensional cephalometric landmarks on three-dimensional computed tomography (3D-CT) surface rendering using clinical protocols based on low-dose (35-mAs) spiral CT and cone-beam CT (I-CAT). The absorbed dose levels for radiosensitive organs in the maxillofacial region during exposure in both 3D-CT protocols were also assessed.
Materials and methods The study population consisted of ten human dry skulls examined with low-dose CT and cone-beam CT. Two independent observers identified 24 cephalometric anatomic landmarks at 13 sites on the 3D-CT surface renderings using both protocols, with each observer repeating the identification 1 month later. A total of 1,920 imaging measurements were performed. Thermoluminescent dosimeters were placed at six sites around the thyroid gland, the submandibular glands, and the eyes in an Alderson phantom to measure the absorbed dose levels.
Results When comparing low-dose CT and cone-beam CT protocols, the cone-beam CT protocol proved to be significantly more reproducible for four of the 13 anatomical sites. There was no significant difference between the protocols for the other nine anatomical sites. Both low-dose and cone-beam CT protocols were equivalent in dose absorption to the eyes and submandibular glands. However, thyroid glands were more irradiated with low-dose CT.
Conclusions Cone-beam CT was more reproducible and procured less irradiation to the thyroid gland than low-dose CT.

Electronic supplementary material The online version of this article (doi:10.1007/s00784-012-0688-2) contains supplementary material, which is available to authorized users.

R. Olszewski · H. Reychler
Department of Oral and Maxillofacial Surgery, Cliniques Universitaires Saint Luc, Université Catholique de Louvain, Brussels, Belgium

L. Frison
Department of Maxillofacial Surgery, CH Lapeyronie, Montpellier, France

M. Wisniewski
Department of Oral and Maxillofacial Surgery, Medical University of Warsaw, Warsaw, Poland

J. M. Denis · S. Vynckier
Department of Oncology and Radiotherapy, Cliniques Universitaires Saint Luc, Université Catholique de Louvain, Brussels, Belgium

G. Cosnard
Department of Medical Imaging, Cliniques Universitaires Saint Luc, Université Catholique de Louvain, Brussels, Belgium

F. Zech
Department of Internal Medicine, Cliniques Universitaires Saint Luc, Université Catholique de Louvain, Brussels, Belgium

R. Olszewski (✉)
Department of Oral and Maxillofacial Surgery, Oral and Maxillofacial Surgery Research Lab, Cliniques Universitaires Saint Luc, Université Catholique de Louvain, Av. Hippocrate 10, 1200, Brussels, Belgium
e-mail: raphael.olszewski@uclouvain.be

Clinical relevance Cone-beam CT should be preferred over low-dose CT for developing three-dimensional bony cephalometric analyses.

Keywords Cone-beam computed tomography · Three-dimensional imaging · Cephalometry · Dosimetry · Maxillofacial

Introduction

Many definitions of "three-dimensional cephalometric analysis" currently exist. Some authors combine separate measurements from the axial, coronal, and sagittal planes (cephalograms) to determine the degree of a patient's craniofacial asymmetry [1, 2]. This approach has been called "two and a half dimensional" (2.5D) as it does not allow for the complete determination of anatomical reality in three dimensions. A method combining two-dimensional frontal and sagittal cephalograms produced from three-dimensional (3D) computed tomography (CT) with a 3D reconstruction of the skull was introduced by Swennen [3]. In Swennen's method, landmarks can be chosen either on frontal and sagittal cephalograms or directly on a 3D skull reconstruction. Adjustment of the position of each landmark both on the cephalograms and on the 3D skull reconstruction is limited. This method is currently restricted to the use of common two-dimensional (2D) cephalometric landmarks. Other 3D cephalometric analyses have been proposed based on measurements between landmarks directly chosen on 2D CT axial slices [4] or on 3D skull reconstructions [5]. Various anthropological cranial reference landmarks have been suggested in place of 2D cephalometric landmarks for performing 3D measurements on skulls [6–8]. The main problem with such analyses is still the lack of established 3D norms, as it is unethical to develop norms by irradiating healthy subjects. We developed and validated a 3D topological cephalometric analysis (ACRO 3D) based on the transposition and adaptation of Delaire's architectural cephalometric analysis to a third dimension [9, 10]. The ACRO 3D analysis is based on individual identification of craniofacial reference landmarks directly from a 3D CT surface rendering. We proposed three cranial planes (C1–C3) and nine craniofacial planes (F1–F8 and a chin plane) to define the 3D cranial and craniofacial reference frames [10]. The sagittal plane was constructed with lateral cranial and craniofacial landmarks belonging to the trigeminal and optic foramina. To diagnose craniomaxillofacial dysmorphia with ACRO 3D analysis, the user must compare the 3D position of major anatomical structures (e.g., the maxilla and mandible) with the constructed, plane-based, 3D reference frame. The alignment (or lack thereof) of different structures along or inside the reference planes is indicative of the type of dysmorphia present in the craniofacial skeleton. The plane-based reference frame illustrates the optimal 3D position for the maxilla and mandible in relation to individual craniofacial characteristics. Defining this optimal 3D position is of extreme importance in orthognathic surgery in which surgeons must correct complex asymmetric faces in all three dimensions [10]. In a previous article, we introduced the use of a clinical low-dose CT protocol for 3D-CT cephalometric applications [11, 12]. However, with the widespread use of the cone-beam CT technique on the oral and maxillofacial areas [13], a comparison between low-dose and cone-beam CT protocols was conducted to determine the most appropriate radiological technique for 3D cephalometry. The hypotheses to be tested were that low-dose CT was more reproducible than cone-beam CT and that both imaging techniques were similar in dose absorption for radiosensitive organs. Therefore, the aim of this article was twofold: (1) to measure and compare the reproducibility of manually picking the osseous reference landmarks on 3D-CT surface renderings from low-dose CT and cone-beam CT using already described landmarks ("m", "na", "fro", "fm", "fz", "dc", "apt", "sof", "pht") [4, 6–8, 10, 11, 14], new 3D cephalometric landmark ("pef"), and alternative positions of the same cephalometric landmark "pterygoid inferior" ("ptia", "ptib", "ptic") [10, 11, 14]; (2) to measure the absorbed dose levels for radiosensitive organs in the maxillofacial area during the exposure for both low-dose and cone-beam CT protocols with an Alderson phantom [11].

Materials and methods

The authors have considered the ethical aspects of their research and ensured that the work did not require the approval of the local ethics committee.

Methodology for the accuracy measurements

Ten human dry skulls without mandibles were scanned in a standard head position with two clinical radiological protocols: medical low-dose spiral CT (Brillance 64, Philips, Eindhoven, the Netherlands) and I-CAT cone-beam CT (Imaging Sciences International, Hatfield, PA, USA). The low-dose CT protocol [11] involved a 1-mm slice with a 512×512 matrix and a 210-mm field of view at 120 kV and 35 mAs. During the low-dose CT protocol, a topogram was also generated (80 kV, 30 mAs, 3.1 s). The parameters for the cone-beam CT clinical protocol were 120 kV, 36.9 mAs, 40 ms, a 160×210-mm field of view and a reconstruction voxel of 0.3 mm. The scanning limits for low-dose CT and cone-beam CT were the same and included the areas from the chin to the vertex of the head.

All native data were saved on CD (DICOM format) and 3D reconstructions were performed with Maxilim software (Medicim, Mechelen, Belgium). The 3D surface rendering

was based on the marching cubes algorithm [15]. Two experienced oral and maxillofacial surgeons participated in this study as independent observers. Each of the observers identified and used a mouse to manually define 24 osseous landmarks on each 3D surface rendering (Table 1; Figs. 1, 2, 3). Eleven bilateral landmarks ("apt", "dc", "sof", "fm", "fro", "fz", "m", "pef", "ptia", "ptib" and "ptic") and two unilateral midline landmarks ("na" and "pht") were identified. Each observer made two series of landmark identifications for both protocols and for all ten dry skulls. The observations were separated by 1 month. The observers were not aware of the radiological protocols used when they identified the landmarks. The 3D coordinates (x, y and z) for each cranial landmark were automatically saved with the Maxilim software.

Statistical analysis methodology

The observers evaluated the position of 24 anatomic cephalometric landmarks for each skull and each method in 3D space. To estimate the accuracy of the two methods, we focused on the reproducibility of the positioning of an anatomical landmark in 3D space. The actual position for each identified landmark was unknown. We posit that the measured landmarks were normally distributed (i.e., formed a Gaussian distribution) with a standard deviation "s" in 3D space in relation to the actual position of the landmark. We did not hypothesise about the actual position of the landmark to be measured, simply calculating the distances between measured landmarks in relation to the observer (inter-observer) and to the observation (intra-observer) in question (Fig. 4). However, when measured landmarks are distant from an actual landmark with a normally distributed (a Gaussian distribution) error, the mean of the distances between the measured and actual landmarks is equal to the mean of the distances between successive measurements of measured landmarks divided by 1.221 (Fig. 4). To estimate the distance of measurements in relation to the actual landmark position, all of the values in the tables must be divided by 1.221. The mean distances between the successive measurements in three-dimensional space are directly related to "s" according to the following formula:

Mean distance

$$= \int_0^{\infty}\int_0^{\infty}\int_{-1}^{1} \sqrt{y^2+z^2-2.y.z.k}\,\frac{e^{-\frac{y^2}{2.s^2}}.e^{-\frac{z^2}{2.s^2}}}{\pi.s^2}\quad \partial k\,\partial y\,\partial z = 1.221s$$

"s" mean distance/1.221.

The standard error of the mean distances was 0.7134 s. All of the values listed in the tables can be divided by 1.221 to give an estimation of the standard deviation of the dispersion around the actual position of the landmarks (Fig. 4). The distances between localisations of the same landmark were based on linear regression by generalised estimating equations (GEE), using quasi-likelihood estimation [16]. The canonical link for the dependent variable y as a function of the independent parameter x is an inverse negative relationship, $y=-1/(\beta_0+\beta_1.x_1+\beta_2.x_2\ \ldots)$, for data presenting a variance proportional to the square of the mean. We computed the covariance matrix by the quasi-least-squares

Table 1 Landmark definitions

Landmark name	Definition
Apex temporalis, "apt" (right, left)	Apex of the petrous portion of the temporal bone
Dacryon, "dc" (right, left)	Top of the lacrimal bone
Foramen rotundum, "fro" (right, left)	Inferior wall of foramen rotundum close to the pterygomaxillary fissure
Frontomaxillary, "fm" (right, left)	Intersection between the posterior ridge of the frontal process of the maxilla with the frontal bone
Frontozygomatic, "fz" (right, left)	Intersection between the zygomatic process of the frontal bone with the frontal process of the zygomatic bone
Landmark M, "m" (right, left)	Intersection of the maxillar, nasal and frontal sutures
Medial superior orbital fissure, "sof" (right, left)	Most inferior point of the superior orbital fissure
Nasion, "na"	Intersection of the nasal and frontal sutures at the midline
Posterior ethmoid foramen, "pef" (right, left)	Intersection between body of the sphenoid bone with the cribriform plate of the ethmoid bone and with the small wing of the sphenoid bone
Pharyngeal tubercle, "pht"	Top of the tubercle on the occipital bone
Pterygoid inferior of type "a", "ptia" (right, left)	Intersection between the palatine bone and the medial pterygoid plate of the sphenoid bone
Pterygoid inferior of type "b", "ptib" (right, left)	Inferior point of the pterygomaxillary fissure
Pterygoid inferior of type "c", "ptic" (right, left)	Superior point of the pterygomaxillary fissure

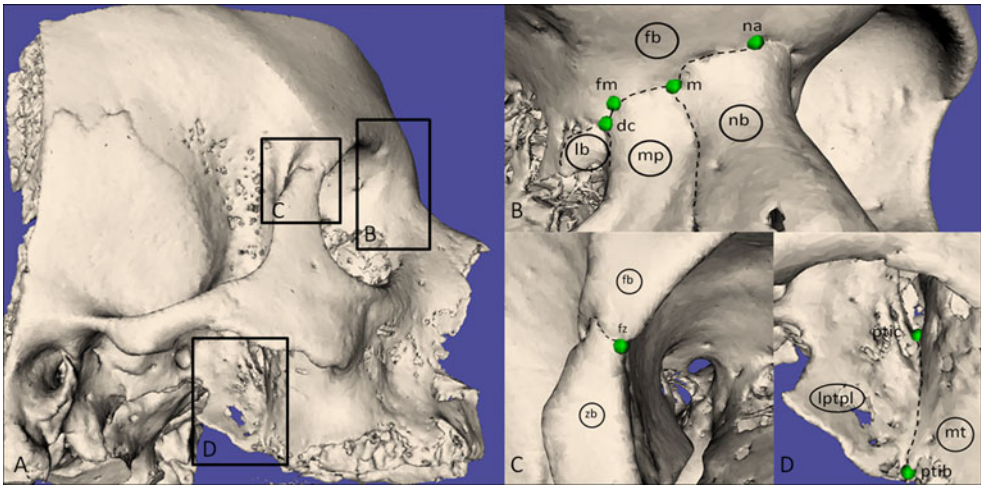

Fig. 1 **a** Lateral view of the skull with regions of interest (*B–D*). **b** Landmarks: *na* nasion, *m*, right, *fm* frontomaxillary, right; *dc* dacryon, right; structures: *nb* nasal bone, *mp* maxillary process of maxilla, *lb* lacrimal bone. Sutures are *underlined* with *dashed lines*. **c** Landmark *fz* frontozygomatic, right; strucures: *fb* frontal bone and *zb* zygomatic bone. **d** Landmarks: *ptib* pterygoid inferior of type "b" and *ptic* pterygoid inferior of type "c". The *dashed line* underlines the pterygomaxillary suture

method [17] because the values are probably correlated for the same skull and the same landmark. To measure inter-observer differences, we calculated a correlation coefficient for the observations from the low-dose CT technique, a correlation coefficient for the observations from the cone-beam CT technique, and a common correlation coefficient for the observations from both techniques. The intra-observer differences were not correlated. All intra-observer differences were incorporated into a common regression, and all the inter-observer differences were incorporated into a separate common regression. It has been shown that the significance of the results from GEE is only valid asymptotically and only if the correlation matrix is strictly appropriate [18]. Therefore, we used a sandwich variance matrix augmented by the correction proposed by Morel, Bokossa and Neerchal [18], which may be evaluated by a normal distribution. The linear regression provides the coefficients that link the dependent variables with the independent variables and also provides the covariance matrix of these coefficients. For sets of multiple comparisons derived from the same regression, we first calculated the crude individual significances, and in a second run, we calculated the adjusted significances according to Holm's sequentially rejective Bonferroni procedure [19]. All of the *p* values are two-sided.

Methodology for dose measurements

For the dosimetric measurements, 100 thermoluminescent lithium-fluoride dosimeter (TLD-100) chips (Harshaw Bicron, Solon, OH) were used. Prior to the measurements, the TLDs were annealed for 60 min at 400°C and for 180 min at 100°C. X6 photons from the SL75 ELECTRA Medical Linac source were used during calibration, and the correction for temperature and atmospheric pressure was

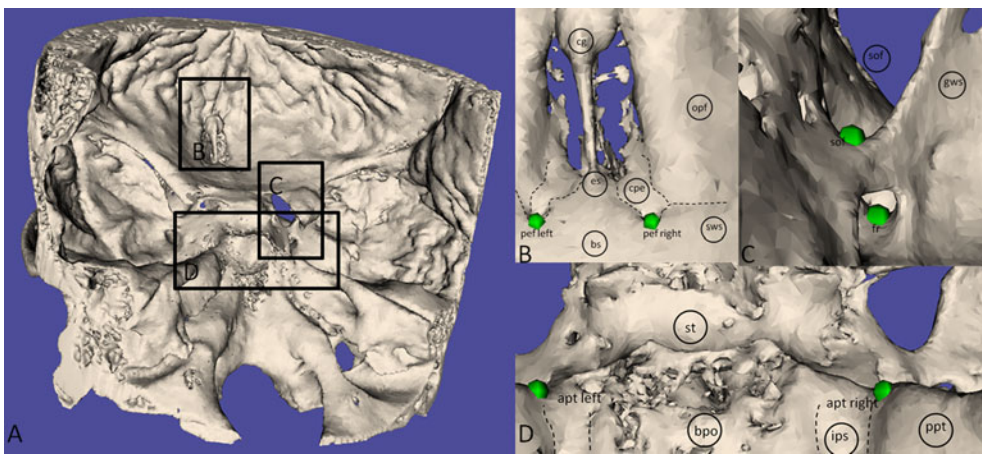

Fig. 2 **a** Posterior view of the skull with regions of interest (*B–D*). **b** Landmarks *pef* posterior ethmoid foramen, right and left; structures: *cg* crista galli process, *es* ethmoid spine, *cpe* cribriform plate of the ethmoid, *opf* orbital plate of the frontal bone, *bs* body of the sphenoid bone and *sws* small wing of the sphenoid bone. **c** Landmarks: *sof* superior orbital fissure, right; *fr* foramen rotundum, right; structures: *sof* superior orbital fissure, *gws* great wing of the sphenoid bone. **d** Landmarks: *apt* apex of the petrous portion of the temporal bone, right and left; structures: *st* sella turcica, *bpo* basilar portion of the occipital bone, *ips* inferior petrous sinus and *ppt* petrous portion of the temporal bone

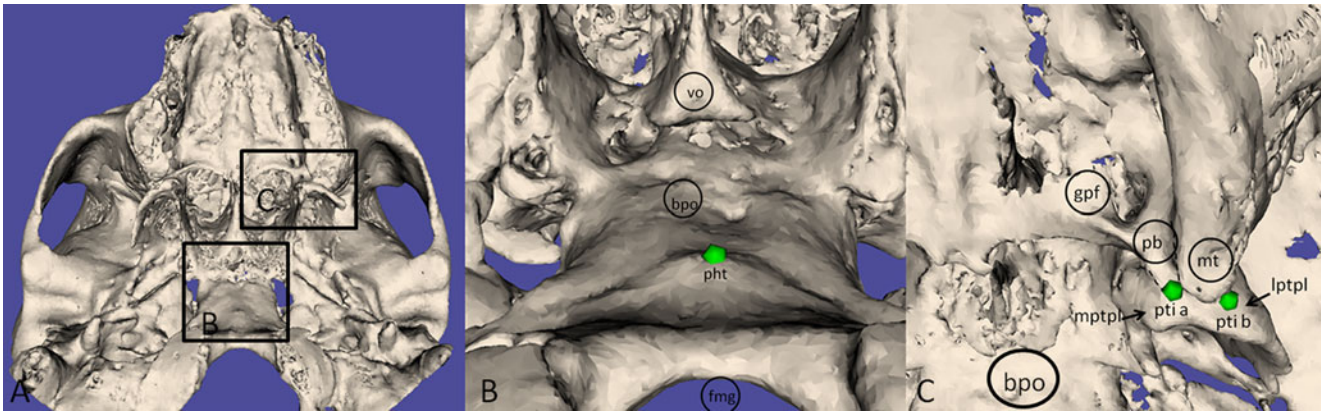

Fig. 3 Inferior view of the skull with regions of interest (*B*, *C*). **b** Landmarks: *pht* pharyngeal tubercle; structures: *fmg* foramen magnum, *bpo* basilar portion of the occipital bone, *vo* vomer. **c** Landmarks *ptia* right pterygoid inferior of type "a", *ptib* right; structures: *mt* maxillary tuberosity, *pb* palatine bone, *gpf* great palatine foramen, *lptpl* lateral pterygoid plate, *mptpl* medial pterygoid plate

also applied. The TLDs were read with a Harshaw reader (Harshaw Bicron, Solon, OH) that uses nitrogen heating, and a correction for background radiation was performed [11]. A total of 100 TLDs were initially calibrated with 100 cGy (beam of 20×20 cm^2). Five series of irradiation, with a lecture at low gain, and annealing were performed for all 100 TLDs. Overall, 50 of the 100 readings from the dosimeters fell within 1% of the mean reading. A second calibration was performed for these 50 TLDs using 1 cGy and a lecture at high gain. Calibration factors were obtained for each of these 50 TLDs. Absorbed organ doses (mGy) were measured using an anthropomorphic Alderson phantom (The Phantom Laboratory, New York, NY) loaded with TLDs. To position the TLDs in the phantom, the sections were separated, and the TLDs were placed in the holes corresponding to the locations of the different organs. One TLD was placed into each hole. Six TLDs were placed in the phantom head in the locations representing radiosensitive sites: the thyroid glands (two TLDs), the submandibular glands (two TLDs), and the eyes (two TLDs). The phantom head loaded with TLDs was exposed three times to the low-dose CT protocol (lecture at high gain), and three times to the cone-beam CT protocol (lecture at high gain). The scanning limits for low-dose CT and cone-beam CT were the same and included the area from the chin to the vertex of the head. After each radiographic exposure, the six exposed TLDs were replaced by six TLDs that had not yet been irradiated. All 50 exposed TLDs (previously calibrated with 1 cGy) were read with the Harshaw reader (Harshaw Bicron, Solon, OH).

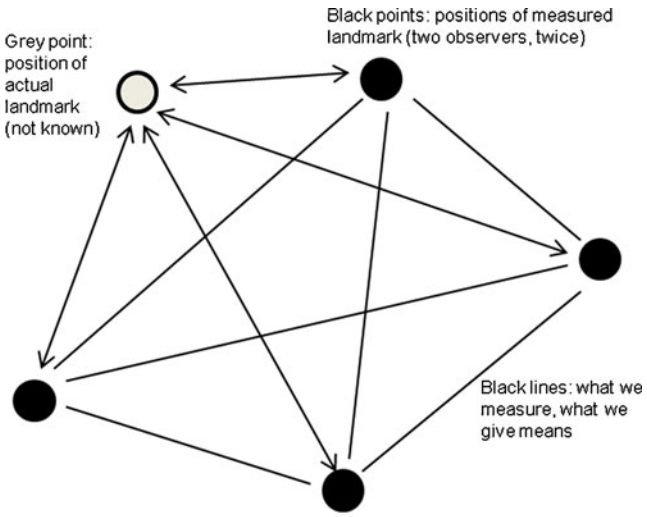

Fig. 4 Methodology overview. Relationship between measured landmarks and actual landmark positions

Results

For measurement of the intra-observer mean distances in both protocols, we used two (for each of the two unilateral landmarks) or four (for each of the 11 bilateral landmarks) distances measured for each site and each skull. Because we used ten skulls and two protocols, there were a total of 960 measurements performed. The intra-observer mean distances for both protocols and for the different sites are presented in Table 2. Intra-observer mean distances were consistently smaller with cone-beam CT than with the low-dose CT protocol (p=0.000075). However, intra-observer mean distances were smaller for two of the 13 sites ("ptia" and "ptib") with the low-dose CT protocol. There was a highly significant interaction between the protocol and the anatomical site (p=0.00002). For the measurement of the inter-observer mean distances in both protocols, we used four (for each of the two unilateral landmarks) or eight (for each of the eleven bilateral landmarks) distances

Table 2 Intra-observer mean distances

Site	Low dose CT	Cone beam CT	Difference (*p*)	*P* corrected
"apt"	1.456±0.138	1.420±0.168	0.86 NS	NS
"dc"	2.148±0.270	1.314±0.146	0.0041	$p<0.05$
"fro"	0.825±0.148	0.994±0.140	0.43 NS	NS
"fm"	2.243±0.258	1.177±0.194	0.0069	NS
"fz"	0.764±0.109	0.551±0.064	0.072 NS	NS
"m"	2.206±0.271	1.017±0.156	0.0010	$p<0.02$
"sof"	1.628±0.216	1.229±0.167	0.15 NS	NS
"na"	1.191±0.245	0.487±0.063	0.0001	$p<0.002$
"pef"	1.624±0.288	0.613±0.124	0.0035	$p<0.04$
"pht"	0.493±0.081	0.828±0.243	0.092 NS	NS
"ptia"	3.026±0.422	3.438±0.420	0.50 NS	NS
"ptib"	4.250±0.511	4.391±0.596	0.86 NS	NS
"ptic"	1.042±0.237	0.676±0.139	0.16 NS	NS

The measurements are expressed as the intra-observer mean distance ± standard error of the mean (in millimeters). See Table 1 for key to abbreviations

NS non-significant

measured for each site and each skull. Because we used ten skulls and two protocols, there were 1,920 measurements performed in total. The inter-observer mean distances for both protocols and for the different sites are presented in Table 3. The inter-observer mean distances were generally smaller with the cone-beam CT than with the low-dose CT protocol ($p=0.00087$). There was a significant interaction between the protocol and the anatomical site ($p=0.045$). The mean absorbed doses for the radiosensitive organs are presented in Table 4.

Table 3 Inter-observer mean distances

Site	Low dose CT	Cone beam CT	Difference (*p*)	*P* corrected
"apt"	2.541±0.204	2.471±0.248	0.77 NS	NS
"dc"	2.522±0.315	1.469±0.122	0.0003	$p<0.0004$
"fro"	1.503±0.190	1.796±0.316	0.37 NS	NS
"fm"	2.075±0.239	1.334±0.187	0.0069	NS
"fz"	1.486±0.148	1.073±0.199	0.15 NS	NS
"m"	2.039±0.281	1.382±0.207	0.044	NS
"sof"	1.652±0.154	1.278±0.136	0.053 NS	NS
"na"	1.392±0.297	1.013±0.244	0.30 NS	NS
"pef"	1.860±0.212	1.110±0.160	0.0028	$p<0.04$
"pht"	0.794±0.262	0.963±0.210	0.50 NS	NS
"ptia"	3.383±0.337	3.632±0.353	0.48 NS	NS
"ptib"	4.310±0.251	4.383±0.265	0.81 NS	NS
"ptic"	1.385±0.419	0.785±0.142	0.092 NS	NS

The measurements are expressed as the inter-observer mean distance± standard error of the mean (in millimeters). See Table 1 for key to abbreviations

NS non-significant

Discussion

The starting point for each "true" (i.e., not 2.5D or 2D) 3D cephalometric measurement-based or topology-based analysis is the individual identification of craniofacial reference landmarks based directly on a 3D-CT or cone-beam CT surface rendering [3, 5, 10, 20]. The landmarks chosen for building the 3D analysis can originate from 2D cephalometry if adapted to the third dimension [3]. For example, there exists one landmark "m" described by Enlow [9, 21] as the intersection of the nasal and frontal sutures found on 2D lateral cephalograms. However, in 3D, there are two "m" landmarks: "m" right and "m" left. The same duplications in 3D space occur with the "fm" (frontomaxillary suture) landmark referenced by Delaire [9]. Such 3D cephalometric landmarks can also be selected from classic anthropological craniofacial landmarks, such as the dacryon or lacrimal bone, "dc" (right and left); foramen rotundum, "fro" (right and left); frontozygomatic suture, "fz" (right and left); nasion, "na"; superior orbital fissure, "sof" (right and left); the apex of the petrous portion of the temporal bone, "apt" (right and left); and the pharyngeal tubercle, "pht" [4, 6–8]. Finally, the 3D approach also allows researchers to test for new 3D craniometric landmarks (e.g., the posterior ethmoid foramen, "pef") that do not exist in 2D cephalometry or for alternative positions ("ptia", "ptib", "ptic") for previously described 3D cephalometric landmarks (e.g., the landmark pterygoid inferior, "pti").

When comparing the reproducibility of craniofacial landmarks for both clinical radiological protocols, there were four landmarks ("dc", "fm", "m" and "pef") for which the cone-beam CT protocol proved to be significantly better than the low-dose CT protocol. These four landmarks belong to small complex areas of suture intersections ("fm" and "m"), to thin bone structures such as the lacrimal bone ("dc") and to the limit between the sphenoid and ethmoid planum ("pef"). The difference in reproducibility between the protocols can be explained by the difference in slice thickness of low-dose CT (1 mm) and cone-beam CT (0.3-mm voxel) used in this study.

Table 4 Absorbed doses (in milligrey) to different organs with cone-beam and low-dose CT using the Alderson phantom head

Sites	Cone-beam CT	Low-dose CT
Eye	5.01	4.84
Submandibular gland	3.30	5.60
Thyroid gland	0.7	3.85

It is certainly possible to use slices thinner than 1 mm for spiral CT to improve the quality of the 3D-CT reconstruction. But the use of more slices will increase the absorbed dose for the patient. Therefore, for this study, we used a previously validated and published protocol with 1-mm slices and 35 mAs [11]. There was no significant difference between both protocols for the other nine anatomical sites. The regrouping of cephalometric landmarks to four categories based on reproducibility [14] (Table 5) showed that ten of 13 landmarks used for the cone-beam CT protocol present very high and high inter-observer reproducibility. However, 11 of 13 landmarks used for low-dose CT present high and average inter-observer reproducibility. Therefore, cone-beam CT may be preferred over low-dose CT by clinicians developing 3D cephalometric dimensional (distance measurements) and topological (3D reference frames) analyses based on the following landmarks: "pht", "ptic", "dc", "sof", "fm" "fro", "fz", "m", "pef" and "na". The results from Tables 2, 3 and 5 show that the reproducibility of the identification of the landmarks "ptia" and "ptib" is low, independent of the radiological protocol used. Landmarks belonging to sites "ptia" and "ptib" should definitively be discarded from studies of 3D cephalometric landmarks. Only the landmark "ptic" might be used in further 3D cephalometric topological analyses and could serve as the posterior and lateral limit of the maxilla.

The maintenance of image quality, despite the reduction in dose, with decreasing tube voltage and/or tube current has already been described [12]. Some authors have compared cone-beam CT with panoramic X-ray [13, 22], frontal radiography [23], multi-slice CT [13, 24] or another cone-beam CT protocol [13, 25, 26]. However, no studies have compared the accuracy of 3D cephalometric landmark identification on 3D-CT surface renderings with low-dose CT and cone-beam CT protocols. The results from Table 4 show that the low-dose CT and cone-beam CT protocols present an equivalent dose absorption for the eyes and submandibular glands. There exists, however, a difference in the absorbed doses at the level of the thyroid gland. For a low-dose CT protocol, the thyroid gland seems to be inside the field of view even if it was excluded (Alderson phantom chin to vertex field of view). Two concomitant explanations could exist for that result: initialisation of the helicoidal movement below the chin of the Alderson phantom and positioning of the TLDs in the most cranial part of the thyroid gland. From a clinical point of view, the irradiation of the thyroid gland could be more important in vivo in low-dose CT because of the extension of the head (not existing in the Alderson phantom), which provides significant exposure of the thyroid gland during the scanning time. For the cone-beam CT protocol, scatter radiation was measured at the level of the thyroid gland. Compared with the ICRP 2007 [27], the thyroid gland has the highest tissue-weighting factor (0.04) in the oral and maxillofacial region because of its high cancer risk in childhood. Therefore, to protect the thyroid gland, a shield with a lead collar should be used in both low-dose and cone-beam CT protocols.

Finally, we presented a statistical methodology for identification of the best reproducible craniofacial anatomic areas for the low-dose and cone-beam CT protocols. The hypothesis to be tested was that the low-dose CT protocol was more reproducible than the cone-beam CT, and it was rejected. Cone-beam CT seems to be a promising image modality for 3D cephalometric analyses using bone-based landmarks. The hypothesis that both imaging techniques were similar in dose absorption for radiosensitive organs was accepted for eye and submandibular glands and rejected for thyroid glands. Moreover, the risk of irradiation to the thyroid gland by full-head cone-beam CT protocol was not null. As the cone-beam CT is more frequently used in children for orthodontic reasons [28, 29], in craniofacial

Table 5 Classification of 3D cephalometric landmarks according to inter-observer reproducibility

Very high inter-observer reproducibility (mean log of distance and SEM<1 mm)	High inter-observer reproducibility (mean log of distance and SEM between 1 and 2 mm)	Average inter-observer reproducibility (mean log of distance and SEM between 2 and 3 mm)	Low inter-observer reproducibility (mean log of distance and SEM > 3 mm)
"pht" (both protocols)	"dc" (cone-beam CT protocol)	"apt" (both protocols)	"ptia" (both protocols)
"ptic" (cone-beam CT protocol)	"sof" (both protocols)	"dc" (low-dose CT protocol)	"ptib" (both protocols)
	"fm" (cone-beam CT protocol)	"fm" (low-dose CT protocol)	
	"fro" (both protocols)	"m" (low-dose CT protocol)	
	"fz" (both protocols)		
	"m" (cone-beam CT protocol)		
	"pef" (both protocols)		
	"na" (both protocols)		
	"ptic" (low-dose CT protocol)		

SEM standard error of the mean

growth assessment [30], and in cleft palate patients [31], a shielding with a lead collar should be utilised during all full-head cone-beam CT protocols.

Conflict of interest The authors declare no conflict of interest.

Disclosure There was no funding for this study.

References

1. Grayson B, Cutting C, Bookstein FL, Kim H, McCarthy JG (1988) The three-dimensional cephalogram: theory, technique, and clinical application. Am J Orthod Dentofacial Orthop 94:327–337
2. Adams GL, Gansky SA, Miller AJ, Harrell WE Jr, Hatcher DC (2004) Comparison between traditional 2-dimensional cephalometry and a 3-dimensional approach on human dry skulls. Am J Orthod Dentofacial Orthop 126:397–409
3. Swennen GR, Schutyser F, Barth EL, De Groeve P, De Mey A (2006) A new method of 3-D cephalometry Part I: the anatomic Cartesian 3-D reference system. J Craniofac Surg 17:314–325
4. Richtsmeier JT, Paik CH, Elfert PC, Cole TM 3rd, Dahlman HR (1995) Precision, repeatability, and validation of the localization of cranial landmarks using computed tomography scans. Cleft Palate Craniofac J 32:217–227
5. Donatsky O, Hillerup S, Bjorn-Jorgensen J, Jacobsen PU (1992) Computerized cephalometric orthognathic surgical simulation, prediction and postoperative evaluation of precision. Int J Oral Maxillofac Surg 21:199–203
6. Cavalcanti MG, Haller JW, Vannier MW (1999) Three-dimensional computed tomography landmark measurement in craniofacial surgical planning: experimental validation in vitro. J Oral Maxillofac Surg 57:690–694
7. Cavalcanti MG, Rocha SS, Vannier MW (2004) Craniofacial measurements based on 3D-CT volume rendering: implications for clinical applications. Dentomaxillofac Radiol 33:170–176
8. Farkas LG, Katic MJ, Forrest CR, Alt KW, Bagic I, Baltadjiev G, Cunha E, Cvicelova M, Davies S, Erasmus I, Gillet-Netting R, Hajnis K, Kemkes-Grottenthaler A, Khomyakova I, Kumi A, Kgamphe JS, Kayo-Daigo N, Le T, Malinowski A, Negasheva M, Manolis S, Ogeturk M, Parvizrad R, Rosing F, Sahu P, Sforza C, Sivkov S, Sultanova N, Tomazo-Ravnik T, Toth G, Uzun A, Yahia E (2005) International anthropometric study of facial morphology in various ethnic groups/races. J Craniofac Surg 16:615–646
9. Delaire J, Schendel SA, Tulasne JF (1981) An architectural and structural craniofacial analysis: a new lateral cephalometric analysis. Oral Surg Oral Med Oral Pathol 52:226–238
10. Olszewski R, Zech F, Cosnard G, Nicolas N, Macq B, Reychler H (2007) 3D CT cephalometric craniofacial analysis: experimental validation in vitro. Int J Oral Maxillofac Surg 36:828–834
11. Olszewski R, Reychler H, Cosnard G, Denis JM, Vynckier S, Zech F (2008) Accuracy of three-dimensional (3D) craniofacial cephalometric landmarks on low-dose 3D computed tomography. Dentomaxillofac Radiol 37:261–267
12. Connnor SEJ, Arscott T, Berry J, Greene L, O'Gorman R (2007) Precision and accuracy of low-dose CT protocols in the evaluation of skull landmarks. Dentomaxillofac Radiol 36:270–276
13. De Vos W, Casselman J, Swennen GR (2009) Cone-beam computerized tomography (CBCT) imaging of the oral and maxillofacial region: a systematic review of the literature. Int J Oral Maxillofac Surg 38:609–625
14. Olszewski R, Tanesy O, Cosnard G, Zech F, Reychler H (2010) Reproducibility of osseous landmarks used for computed tomography based three-dimensional cephalometric analyses. J Craniomaxillofac Surg 38:214–221
15. Lorensen WE, Cline HE (1987) Marching cubes: a high resolution 3D surface construction algorithm. Comp Graph 21:163–169
16. McCullagh P (1983) Quasi-likelihood functions. Ann Stat 11:59–67
17. Chaganty NR, Shults J (1999) On eliminating the asymptotic bias in the quasi-least squares estimate of the correlation parameter. J Stat Plan Inf 76:145–161
18. Morel JG, Bokossa MC, Neerchal NK (2003) Small sample correction for the variance of GEE estimators. Biometric J 45:395–409
19. Larzelere RE, Mulaik SA (1977) Single-sample tests for many correlations. Psychol Bull 84:557–569
20. Van Cauter S, Okkerse W, Brijs G, De Beule M, Braem M, Verhegghe B (2010) A new method for improved standardisation in three-dimensional computed tomography cephalometry. Comput Methods Biomech Biomed Engin 13:59–69
21. Enlow DH (1975) Handbook of facial growth. WB Saunders, Philadelphia
22. Ludlow JB, Davies-Ludlow LE, Brooks SL (2003) Dosimetry of two extraoral direct digital imaging devices: NewTom cone beam CT and Orthophos Plus DS panoramic unit. Dentomaxillofac Radiol 32:229–234
23. Van Vlijmen OJ, Maal TJ, Berge SJ, Bronkhorst EM, Katsaros C, Kuijpers-Jagtman AM (2009) A comparison between two-dimensional and three-dimensional cephalometry on frontal radiographs and on cone beam computed tomography scans of human skulls. Eur J Oral Sci 117:300–305
24. Schulze D, Heiland M, Thurmann H, Adam G (2004) Radiation exposure during midfacial imaging using 4- and 16-slice computed tomography, cone beam computed tomography systems and conventional radiography. Dentomaxillofac Radiol 33:83–86
25. Ludlow JB, Davies-Ludlow LE, Brooks SL, Howerton WB (2006) Dosimetry of 3 CBCT devices for oral and maxillofacial radiology: CB Mercuray, NewTom 3 G and i-CAT. Dentomaxillofac Radiol 35:219–226
26. Van Vlijmen OJC, Rangel FA, Bergé SJ, Bronkhorst EM, Becking AG, Kuijpers-Jagtman AM (2010) Measurements on 3D models of human skulls derived from two different cone beam CT scanners. Clin Oral Investig. doi:10.1007/s00784-010-0440-80
27. Boetticher H, Lachmund J, Looe HK, Hoffmann W, Poppe B (2008) 2007 recommendations of the ICRP change basis for estimation of the effective dose: what is the impact on radiation dose assessment of patient and personnel? Rofo 180:391–395
28. Mah JK, Hunag JC, Choo H (2010) Practical applications of cone-beam computed tomography in orthodontics. J Am Dent Assoc 141:7S–13S
29. Cevidanes L, Baccetti T, Franchi L, McNamara JA Jr, De Clerck H (2010) Comparison of two protocols for maxillary protraction: bone anchors versus face mask with rapid maxillary expansion. Angle Orthod 80:799–806
30. Cevidanes LH, Heymann G, Cornelis MA, De Clerck HJ, Tulloch JF (2009) Superimposition of 3-dimensional cone-beam computed tomography models of growing patients. Am J Orthod Dentofacial Orthop 136:94–99
31. Garib DG, Yatabe MS, Ozawa TO, da Silva Filho OG (2011) Alveolar bone morphology in patients with bilateral complete cleft lip and palate in the mixed dentition: CBCT evaluation. Cleft Palate Craniofac J (in press)